# How to guarantee Phase-Synchronicity in Active Load Modulation for NFC and Proximity

Michael Stark
NXP Semiconductor Austria
Austria
michael.stark@nxp.com

Michael Gebhart
NXP Semiconductor Austria
Austria
michael.gebhart@nxp.com

***Abstract*—The introduction of Near Field Communication increases the application domain of RFID systems operating in the 13.56 MHz frequency domain significantly. Especially the environment within a Smartphone or a mobile device makes great demands on the physical characteristics of proximity coupling systems. Recently active load modulation was introduced to overcome the limitations using passive load modulation. However, with this new technology the problem of phase-synchronicity arises. Therefore, contactless Card phase drift test methods have to be developed to guarantee interoperability. This paper discusses the problem of phase synchronicity and analyses the appropriateness of the contactless test set-up. Moreover, we present an algorithm which allows to measure the phase drift accurately and compare results to a proposed algorithm. We will show that our algorithm significantly outperforms the other proposal in terms of phase drift measurement accuracy.**

## I. INTRODUCTION

Near Field Communication (NFC) is an emerging interface for mobile devices like Smartphones and Tablet PC´s. From application perspective, a communication channel for data exchange is opened if two NFC devices get close to each other until they nearly touch. This intuitive user-friendly approach is based on an underlying sophisticated technical process. From technical perspective, NFC uses a contactless interface of an *H*-field alternating at a $fc_{PCD}$ = 13.56 MHz sine-wave carrier frequency. In fact the NFC interface is not limited to NFC-to-NFC device communication but in initiator mode is defined to open a communication channel to contactless cards and labels. Contactless cards are based on secure battery-less transponders and are used in person-related applications like payment, the electronic passport or for access control. Contactless labels on the other hand have applications in logistics and may contain European product code (EPC) information to declare goods.

Moreover, NFC can behave like a contactless card, so the Smartphone or Tablet can replace payment cards or bus tickets, and allow access to secured facilities. Summarizing, NFC is a multi-protocol standard, compatible to most international contactless communication standards in terms of modulation, data format and command set. NFCIP1, defined in [1, 2], consists of the International Proximity Card Standard [3], Type A, 106 kbit/s, and FeliCa [4] at 212 and 424 kbit/s. NFCIP2, defined in [5], extends the protocol set by adding the International Vicinity Standard [6] and [3] Type B (both Reader functionality).

It is well known that NFC utilizes the same physical air interface as the Proximity Card Standard [3]. At the beginning the Proximity Standard was intended for Cards with a loop antenna size to fit into an ID-1 Card format as specified in [7]. Meanwhile this standard gradually became a generic contactless interface for consumer devices. This also changed the requirement of the loop antenna from class 1 antenna size in ID-1 (credit card) format to much smaller and thinner antennas, which should still allow interoperability to all other standard conformant devices. In particular, this is a challenge for the Card to Reader communication which uses the principle of passive load modulation (PLM). Generally, the passive card transmits data synchronously to the Reader *H*-field by a pure change of its load.

The side band amplitude (SBA) defined in [8] is a parameter related to the signal quality. The SBA of battery-less transponders is physically limited by the antenna size [9]. Therefore, PLM is especially a challenge for NFC, as devices like Smartphones offer a completely different environment than Proximity Cards or Readers. However, in contrast to battery-less cards, such devices have external supply power available. In order to overcome the mentioned problem, the idea came up to use the external supply to actively drive current in the antenna. This so called active load modulation (ALM) enhances the Card emulation mode operation.

ALM on the one hand extends the reliable communication to even smaller antenna sizes. On the other hand, during active communication periods of the Card device the Reader *H*-field is not directly observable. This might result in a not synchronous Card response and thus a phase drifting signal received by the Reader. This paper discusses different methods to measure the phase drift (PD) of a Card. Finally, we propose an algorithm to be included into standardized compliance tests.

## II. FUNDAMENTALS

### A. Reader-Card synchronicity

Proximity coupling devices use for communication the master-slave principle. Generally, the Reader is the master and the Card or the device in card mode is the slave. This means that the Reader initiates all activities and the Card just answers. Moreover, the Card has to send its response synchronously to the Reader carrier signal. Specifically, the symbol period

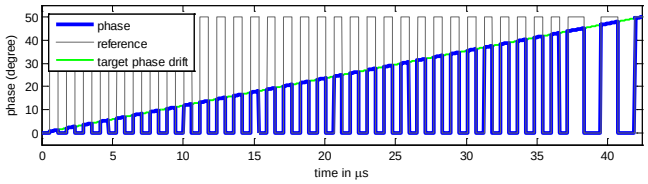


Fig. 1 Illustrations of an unipolar ALM signal with a constant phase drift of 50° over a frame. This corresponds to a frequency error of 817 Hz between Reader and Card.

of the transmitted signal $etu = N \cdot \tau_{PCD}$ is an integer multiple of the Reader carrier period $\tau_{PCD} = 1/fc_{PCD}$. A clock signal synchronous to the Reader can be easily derived by sensing the Reader emitted *H*-field, resulting in $\tau_{PCD} = \tau_{PICC}$, where $\tau_{PICC}$ is the internally used Card carrier period.

However, with the introduction of the ALM for the Card to Reader communication the Reader *H*-field is obscured by the active transmitted Card field. Thus, during the time when the Card actively transmits its response, the Reader *H*-field signal is not directly observable. In this case Reader and Card internal clock sources are not synchronized anymore and the condition that $\tau_{PCD} = \tau_{PICC}$ is violated, resulting in $\tau_{PICC} = \tau_{PCD} \pm \Delta\tau_{PD}$. This term can also be expressed as the inverse of $\tau_{PICC}$, the frequency $fc_{PICC} = fc_{PCD} \pm \Delta f_{PD}$, where $\Delta f_{PD}$ is the frequency error between Reader and Card. Note, for all considerations let us assume that $\Delta f_{PD} << f_{c_{PCD}}$. Generally, a not synchronous Card response can be observed as phase drift in the base band when demodulated with respect to the Reader signal. Apparently, the change of the envelope of the actual phase modulation of the Card equals the phase drift (PD). This is illustrated in Fig. 1 for a fixed $\Delta f_{PD}$. The PD and the frequency error are related as follows:

$$\varphi(t) = 2\pi \int_{-\infty}^{t} f(t)\partial t = 2\pi \int_{-\infty}^{0} f(t)\partial t + 2\pi \int_{0}^{t} f(t)\partial t = \varphi_0 + 2\pi \int_{0}^{t} f(t)\partial t, \quad (1)$$

where *f(t)* is the frequency error and $\varphi_0$ is the initial phase between Reader and Card *H*-field. For a constant frequency error (1) reduces to

$$\varphi = \varphi_0 + 2\pi (f \cdot t + C), \quad (2)$$

where *C* is a constant factor.

### B. Options for Active Load Modulation signal generation

For the Card to Reader communication the Card passively modulates the Reader *H*-field at the subcarrier frequency $f_{sub} = fc_{PICC}/16$ by changing its load accordingly. This results in an AM and/or PM modulated *H*-field observed at the air interface. The goal of ALM is to generate an identical signal at the air interface as PLM by using active modulation. In the following we introduce an option to generate such an ALM modulation. Unipolar ALM modulation emits a signal at $fc_{PICC}$ in phase to the Reader *H*-field during the first half of the subcarrier period. During the second half of the subcarrier period the Card remains mute. Ideally unipolar ALM results in a pure ASK modulated Reader *H*-field. Due to the loosely coupled antenna system, in reality an AM and/or PM modulated *H*-field is observed at the air interface. For this reason this type of modulation is called unipolar modulation.

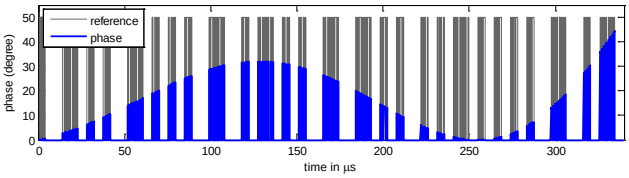


Fig. 2 Plot of a sinusoidal changing PD (blue color) of 50° over a frame with a bit rate Type A, 106 kbit/s. The reference signal is plotted in grey color.

### C. Signal generation with defined phase drift over frame

In order to develop a reliable PD measurement algorithm the generation of a signal with a defined PD over a frame is of major importance. This section discusses the generation of a constant PD signal and one with a sinusoidal changing PD. For the signal generation let us assume to know the frame length, bit rate with according symbol duration as well as a target PD value.

The constant phase drift Card response signal generation is performed as follows:

- The length of the Card frame in seconds is given at the air interface as: $t_F = N_{bits} \cdot etu$, where $N_{bits}$ is the number of bits of the frame and *etu* is the symbol duration. The frequency error with respect to the Reader can be computed by re-arranging (2) to $\Delta f_{PD} = \varphi_{tar}/(2\pi \cdot t_F)$, where $\varphi_{tar}$ is the target PD in radians.
- Generate a channel coded signal from the binary data stream with the new time base $\tau_{PICC} = \tau_{PCD} + \Delta\tau_{PD}$. In digital domain the Card frame is usually generated by changing the time base, i.e., the sampling rate. Finally the Card signal is re-sampled to the Reader sampling frequency.

A sinusoidal changing PD of the Card frame basically performs the same 2 steps as the constant PD with the following differences: Step 1 uses 50% of the actual $t_F$ to achieve the target PD at the end of the frame. In step 2 the time base is changing over time, i.e., $\tau_{PICC}(t) = \tau_{PCD} + \Delta\tau_{PD}(t)$, where $\Delta\tau_{PD}(t)$ is weighted by a sinusoidal as $\Delta\tau_{PD}(t) = \Delta\tau_{PD}\ (\sin(\omega_{CR}t) + 1) \cdot 0{,}5$, where $\omega_{CR}$ is the changing frequency of the PD in radians. $\omega_{CR}$ is computed such that the PD oscillates one full period over the frame. Note, this is just one example to generate a changing PD signal. Fig. 1 shows one example for a constant PD of 50° for an unipolar modulated ALM signal. Fig. 2 shows an unipolar ALM signal with changing PD of 50°.

## III. Compliancy Measurement

### A. ISO/IEC 14443 Type A & B bit representation and coding

A review of the definitions of channel coding for bit representation [3] unveils differences between the protocols and bit rates. Proximity Type A, 106 kbit/s defines Manchester coding by the presence or absence of subcarrier cycles in half of the bit duration. For this bit rate the information is not coded in the phase of the signal. Thus, due to the bit coding

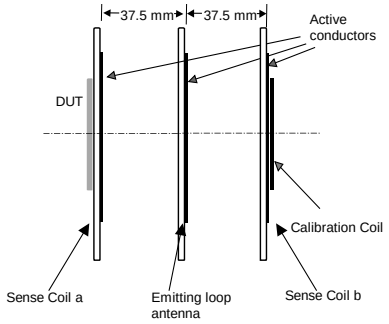


Fig. 3: Coaxial antenna arrangement of the ISO-Setup.

this type is insensitive to phase drift. For higher bit rates of the Type A interface (> 106 kbit/s) and all bit rates of Type B, an absolute bit assignment to the subcarrier phase must be met. Type A defines in the Start-of-Communication (SOC) sequence a burst of 32 subcarrier cycles (phase of logic "1") followed by inverted subcarrier cycles (phase of logic "0") for one bit duration. Type B defines the logic level for NRZ-L coding at the start of a Card frame by the initial phase of the subcarrier.

In essence this means we have to differentiate criterions: A *bit grid violation* concerns all protocols and bit rates, a *bit coding violation* concerns Type A higher bit rates, and all Type B bit rates. This second, harder criterion leads to a maximum limit for allowable phase drift of the Card response, which should be 30° over a complete data frame (including some margin between Card and Reader, and measurement tolerance). This gives the reason to measure the phase drift very accurately, to guarantee interoperability of Cards, Readers, and NFC devices.

### *B. ISO Setup introduction and description*

Complimentary to the base standard, e.g. the Proximity Standard [3], which specifies properties and the signal shape parameter range for the Air Interface, there is a test standard, e.g. the Proximity test standard [8], which specifies a set-up and dedicated methods to measure and verify these values. As there are several base standards for contactless HF communication, there are also several test standards, which can basically be differentiated into two concepts:

One approach follows application-oriented testing. The set-up for Card testing consists of a Reader antenna including the matching network, the so-called proximity coupling device (PCD) and some means to generate and evaluate signals. The Card as device under test (DUT) is measured at dedicated points in a so-called operating volume over the Reader antenna. The set-up for reader testing consists of a so-called Reference Proximity Integrated Circuit Card (Ref-PICC), an emulation of the physical properties of a transponder card antenna circuit. This Ref-PICC is varied in the operating volume of the DUT reader. Examples for this approach are the EMVCo [10] and the NFC Forum [11] test strategy.

The other approach uses sophisticated concepts and a coaxial antenna arrangement, to measure most accurate values. This concept also allows better to differentiate different properties at the air interface from each other, and to find root

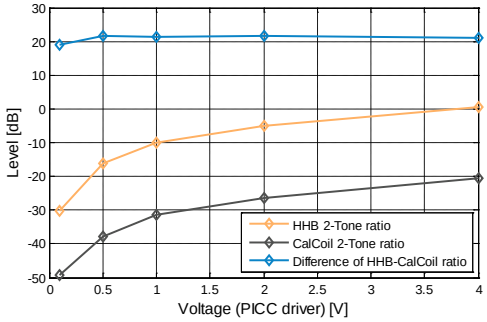


Fig. 4. Two tone cross talk analysis on *ISO set-up*. The orange line shows the two-tone ratio of PICC and PCD signals as measured by the HHB and the black colored line as measured by the CalCoil. The difference between the two ratios is plotted in blue.

causes for communication problems, but it may indeed be less related to the practical use-case. Examples for this approach are the Proximity [8] test setup and NFC test setup [12]. It makes sense to use one of these existing measurement concepts and set-ups for the new phase drift measurement. We will use [8], which is simply called "the ISO set-up", for our considerations.

The coaxial antenna arrangement as shown in Fig. 3 consists of a circular PCD antenna in the center, which emits the *H*-field alternating at $fc_{PCD}$. The DUT is placed in a distance specified to have a homogenous *H*-field distribution for the field component perpendicular to the DUT antenna plane over the size of the DUT. The *H*-field strength is measured as the induced voltage in a so-called calibration coil (CalCoil), in equal distance but at the opposite side of the PCD antenna. Furthermore, two sense coils are placed in equal distance at both sides of the PCD antenna and connected over resistors to a so-called Helmholtz bridge (HHB). This bridge allows to nearly compensate the voltage induced by the primary *H*-field emitted by the PCD antenna, and to measure at relatively good signal to noise ratio the voltage induced by the secondary *H*-field, emitted by the DUT antenna. A detailed description of the set-up can also be found in [13, 14].

In ALM mode, the DUT may emit bursts of a secondary carrier signal at $fc_{PICC}$, which is probably not perfectly synchronous to the primary $fc_{PCD}$ carrier signal over the duration of one data frame. To measure the amount of this phase drift of the secondary versus the primary carrier frequency, it is desirable to have two separate channels, one for the primary and one for the secondary signal. As it seems,

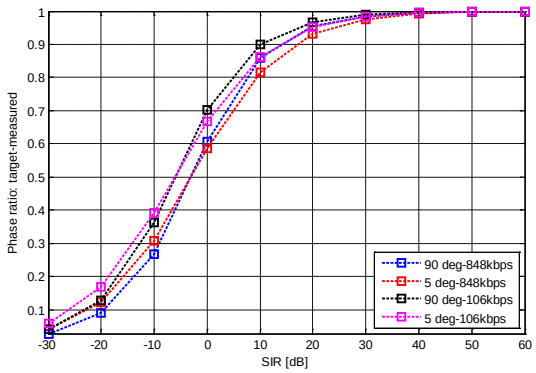


Fig.5. Simulation of the phase ratio between target phase and the phase as measured in the mixture as a function of the signal mixture SIR.

the CalCoil signal (for the primary signal) and the HHB signal (for the secondary signal) should be good candidates for this approach. Unfortunately in practice there are several effects of cross-talk and noise which violate the concept of ideal, separate channels. Therefore, it is necessary to consider and quantify these effects before the choice of an appropriate algorithm for accurate phase drift measurement can be made.

### *C. Cross-talk of DUT and PCD frequencies to CalCoil and HHB signals*

Although the CalCoil is at the opposite side of the PCD antenna than the DUT, there is a connection between the two Sense coils via the HHB. The sense coil close to the DUT (emitting the ALM signal) will pick up this signal, and the current over the resistor bridge flowing through the second sense coil will emit this signal, close to the CalCoil. So the signal captured at the CalCoil is not only the primary PCD carrier signal, but also contains some interference of the secondary ALM transponder signal. Even more critical is the cross-talk of the PCD antenna emitted carrier signal to the HHB. The standard defines to compensate the HHB without DUT (Ref-PICC), before the actual measurement. But as the Ref PICC transponder has a closed, resonant antenna circuit, the primary *H*-field will cause a current in this Ref-PICC antenna, oscillating at the primary carrier frequency, which causes a secondary *H*-field oscillating at the same frequency.

In order to quantify the amount of cross-talk we carried out the following two-tone cross-talk experiment using the ISO set-up: In this experiment the PCD emits a sinusoidal signal at $f_c$ with constant *H*-field and the Ref-PICC emits a sinusoidal at $f_c+f_{sub}$. The two signals are captured, properly terminated by active probes, once with the HHB and once with the CalCoil. Fig. 4 plots the two-tone level ratio as a function of the Ref-PICC driver voltage. The orange colored line shows the ratio between the two signal levels as measured at the HHB and the black colored line as measured at the CalCoil. We observe that the ratio of HHB and CalCoil increases as the driver voltage increase. Moreover, we see that the ratios are parallel to each other regardless of the Ref-PICC voltage. This is shown in Fig.4 by the blue line which plots the difference between the two ratios [16]. We conclude that the cross-talk of the PCD signal to the HHB may impact the PD measurement.

### *D. Signal to interference ratio and phase drift*

In the previous section we have shown that the pure signal as emitted by the Card is not directly observable in the actual setup to perform compliance tests. Instead a mixture consisting of the Reader and the Card *H*-field will be captured by the HHB. This section analyses the impact of a stationary Reader *H*-field on the measured PD of a Card. Therefore, let us assume that we capture an additive mixture of the Reader and Card signal at the HHB. In the following simulation the HHB signal is artificially generated at different signal-to-interference ratios (SIR). For the SIR computation let us assume that the Card signal corresponds to the signal and the Reader signal is the interference. Then the SIR is defined in dB as

$$SIR = 20 \cdot \log_{10}\left(\frac{\delta_S}{\delta_I}\right) \quad [dB], \tag{4}$$

where $\delta_S$ is the Card signal standard deviation and $\delta_I$ is the Reader signal standard deviation. Fig. 5 summarizes the simulation results for the measured PD in dependency of the SIR. In the graph the ratio between the target and the measured PD is plotted as a function of the SIR for a 5° and a 90° PD over a 4 Byte frame at bit rates of Type A, 106 and 848kbit/s. The simulation clearly shows that the measured PD is significantly influenced for SIR values smaller than 20 dB. We will see in the experimental section that the estimated SIR of the HHB signal is in the range of –20 dB. This means that the PD algorithm has to include means to compensate the impact of the Reader signal in order to measure the PD accurately.

In general, there are two options to remove the Reader signal component from the HBB. Firstly, one can decompose the mixture and remove the Reader signal in the HF domain or secondly, demodulate the HHB signal and remove the Reader signal in the complex base band. For HF compensation we note that, generally the Card has a resonant antenna circuit and therefore the secondary *H*-field is phase shifted compared to the primary *H*-field. Thus, the resistive HHB compensation *with DUT* (instead of without) is not possible. Alternatively it would be possible to capture each Sense coil signal separately with the oscilloscope and to compensate the bridge offline, by a phase-shift and a gain-shift. The limiting aspect of this idea is the signal capturing with an oscilloscope, which (according to [8]) should offer at least 500 MS/s and 8 bit amplitude resolution per channel. Since the amplitude of each individual Sense coil signal is much higher than the signal captured from a compensated Helmholtz bridge, this concept is limited by quantization noise. Nevertheless we have taken it into consideration.

Therefore, the investigated HF compensation uses the HHB and the CalCoil signal and performs the compensation in software. For the compensation method we assume that the CalCoil only contains signal components from the Reader. Then one can decompose the additive mixture of the HHB by phase shifting and scaling the CalCoil signal with respect to

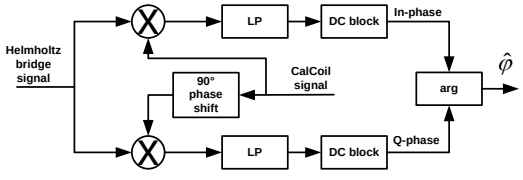


Fig. 6. Illustration of the homodyne demodulation based phase drift algorithm.

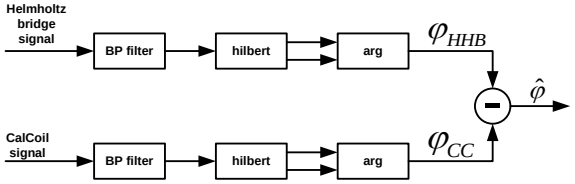


Fig. 7. Illustration of the Hilbert demodulator phase drift algorithm.

the HHB such the HHB signal gets a minimum during a silence time period of the Card. Experiments have shown that by using this method the SIR can be improved by maximum 30 dB from -20 to approximately +10 dB. From Fig. 5 we see that this improvement is not sufficient. Compensation means in the complex base band have more effect, so these have to be applied.

## IV. Investigated Phase Drift Measurement Methods

This section describes different algorithms to measure the phase signal over time as emitted by the Card using the Reader signal as reference. The goal for each algorithm is to measure the phase modulation of the Card with respect to the Reader signal. In the event that the Card internal clock is not locked to the Reader signal, a phase drift will be additionally visible in the phase signal. All presented algorithms use the Helmholtz bridge (HHB) and the CalCoil signals of a complete Card frame response as input signals to compute the phase signal over time as output. Two methods will be discussed in the following, namely, the homodyne demodulator and the Hilbert demodulator algorithms.

### A. Homodyne Demodulator Algorithm

This realization of the homodyne demodulator performs the down conversion to the complex base band of the HHB signal using the CalCoil signal as demodulation signal. The algorithm directly uses the CalCoil signal as In-phase demodulation signal and its 90° shifted version as quadrature (Q) -phase demodulation signal. A 90° phase shifted signal to the CalCoil signal can be computed using an integrator or the Hilbert transform. The use of the CalCoil signal as demodulation signal solves 2 problems at the same time: Firstly, the signal is demodulated with respect to the relative reference, the Reader emitted signal. Secondly, this demodulation approach inherently compensates for the frequency error due to the non synchronous sampling which results in a constant phase drift.

Due to the mixing process the In- and Q-phase signals contain twice the carrier frequency. This unwanted signal component is removed by a moving average type low pass filter. Afterwards the most important step of the algorithm follows. It is the removal of the DC component contained in the In- and Q-phase signal, respectively. This mean component mainly comes from the Reader signal and is proportional to the carrier amplitude. In section III.D we observed that exactly the imperfect separation of Reader and Card signal as captured at HHB and CalCoil significantly influence the measured phase signal over time. Finally, the argument of In- and Q-Phase signal corresponds to the phase modulated signal of the Card over time. Note, this algorithm provides phase information at the Sampling rate. The algorithm is summarized in Fig. 6.

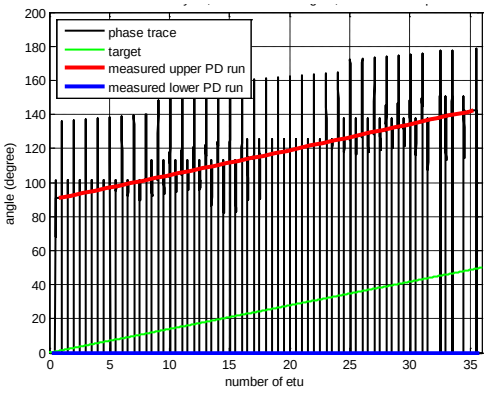


Fig. 8. Simulation results using the homodyne demodulator based algorithm for PD measurement. The green line shows the target PD of 50° over the frame and the black line the actual measured PD by the algorithm.

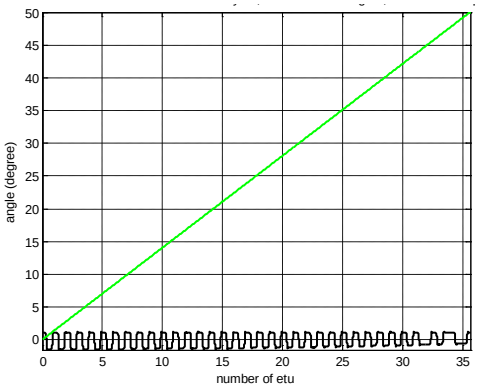


Fig. 9. Simulation results using the Hilbert based algorithm for PD measurement. The green line shows the target PD of 50° over the frame and the black line the actual measured PD.

### B. Hilbert Demodulator Algorithm

The Hilbert based phase drift algorithm to measure the phase of a Card was proposed in [15]. The basic principle of this algorithm is illustrated in Fig. 7. The captured HHB and CalCoil signals are band pass filtered using a second order Butterworth filter with cut-off frequencies at $fc_{PCD}$ ±5 MHz. Afterwards both signals are Hilbert transformed. Subsequently, the argument for each analytic signal is computed resulting in $\varphi_{HBB}$ and $\varphi_{CC}$. Note, these phase signals are rotating with the carrier frequency plus the frequency error due to non synchronous sampling. The final phase signal $\hat{\varphi}$ over time is computed by the difference between $\varphi_{HBB}$ and $\varphi_{CC}$. Computing the difference between the HHB and the CC phase signals alleviates two signal immanent characteristics. Firstly, the phase rotation at *fc* and the frequency error contained in both signals cancel out. Secondly, the HHB signal is measured with respect to the CalCoil signal.

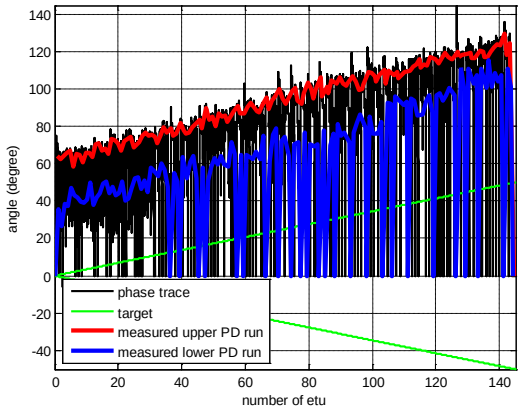


Fig. 10. PD measurement results of the homodyne demodulator algorithm. The green line shows the target PD of 50° over the frame and the black line the actual measured PD by the algorithm.

## V. Simulation and Experimental Results

This experimental section is split into two parts, the first presents simulation and the second real measurement results.

### A. Simulation Results

For this simulation let us assume that the CalCoil signal contains just the Reader *H*-field and the HHB contains a mixture of the Reader and the Card signal. Moreover, let us assume an additive mixture model where the signals are mixed at a known SIR. In the simulation the Card transmits 4 Bytes of data at a bit rate of Type A, 848 kbit/s using unipolar modulation. Moreover, the Card has a fixed frequency error $\Delta f_{PD}=2369.68Hz$ to the Reader. This error corresponds to a constant PD of 50° over the whole frame. This experiment uses a HHB signal mixed at an SIR of –30 dB. Fig 8 and 9 show the results for the homodyne and the Hilbert algorithms. In the 2 figures the measured PD is shown in black color and the target PD in green. The results show that only the homodyne demodulator accurately follows the target PD. The Hilbert algorithm does not compensate for the PCD frequency signal component which results in a reduced PD. The measured PD of the Hilbert based algorithm is approximately 1°. If we multiply this value by the inverse factor of ~0.02 taken from fig. 5 at an SIR of -30 dB then we see that the PD would be in the correct range.

### B. Experimental Results on real Setup

As a last step the performance of the proposed algorithms is assessed on a real PCD1 Test assembly [8]. Both, Reader and Card signal are synchronously emitted using a two channel type arbitrary wave form generator. As Card the Ref PICC was adjusted to the following settings: The Card was tuned to maximum loading with 6 $V_{DC}$ at the (minimum required) *H*-field of 1.5 A/m. The ALM signal was emitted using the pickup coil with an antenna impedance matching to 50 Ω at $fc_{PCD}$. The load modulation was adjusted to produce an upper and lower side band amplitude (SBA) of 12.6 mV(p) and 14.0 mV(p), respectively. Note, these values are selected to be well below the minimum limit SBA for Proximity Cards and thus can be treated as worst case. Also in this experiment the Card emits a PD of 50° over one frame at a bit rate of Type A, 848 kbit/s using unipolar modulation. The HHB and CalCoil signal are captured with a conventional 8 bit resolution and 500 MS/s oscilloscope. Fig. 10 shows the result for the homodyne demodulator algorithm. As in the simulation results the homodyne demodulator algorithm can follow the target PD accurately and the Hilbert algorithm fails due to the missing Reader frequency signal compensation. The Hilbert algorithm measures a similar PD value of 1° as in the simulation. Unfortunately there is no equivalent simple approach to compensate for the Reader signal within the HHB signal as available for the homodyne algorithm.

## VI. Conclusions

In mobile devices the available space is very limited. This also requires that NFC based communication uses smaller antenna form factors. The reduced antenna form factor changes the physical requirements for a stable communication significantly. As a consequence the active load modulation concept for the Card to Reader communication was introduced to overcome this limitation. However, during the active emission of the Card *H*-field the Card can not directly access the pure Reader *H*-field which is fundamental to be synchronous to the Reader. This missing synchronicity between Card and Reader effectively can be observed as phase drifting Card signals. This paper discussed this problem and introduced test methods for compliance tests. All discussed algorithms use the “Proximity” PCD1 Test assembly [8]. The Hilbert based algorithm has been proposed in [15]. We have shown that this algorithm cannot compensate for the influence of the Reader *H*-field on the measured phase drift. In contrast, the proposed homodyne demodulator algorithm compensates for the Reader *H*-field impact in the complex base band. In simulation and real measured we have shown the performance of both algorithms. Only the homodyne demodulator algorithm follows well the actual generated target phase drift.

## References


[1] ECMA340, *Near Field Communication Interface and Protocol -1 (NFCIP-1)*, 2nd ed., Dec. 2004.

[2] ISO/IEC18092:2004, I*nformation technology -- Telecommunications and information exchange between systems -- Near Field Communication -- Interface and Protocol (NFCIP-1)*, ISO, Retrieved 11 Dec. 2011.

[3] ISO/IEC14443: *Identification cards – Contactless integrated circuit cards – Proximity cards.* ISO, Geneva, Switzerland, 2011.

[4] JIS 6319-4:2010, *Specification of implementation for integrated circuit(s) cards -- Part 4: High speed proximity cards*, Japanese Standards Association, 2010

[5] ECMA352, *Near Field Communication Interface and Protocol -2 (NFCIP-2)*, 2nd ed., June 2010

[6] ISO/IEC15693: *Identification cards – Contactless integrated circuit cards – Vicinity cards – Part 2: Air interface and initialisation*. ISO, Geneva, Switzerland, 2006.

[7] ISO/IEC7810:1995: *Identification cards -- Physical characteristics* ISO, Geneva, Switzerland, 2003.

[8] ISO/IEC10373-6: *Identification cards – Test methods – Part 6: Proximity Cards.* ISO, Geneva, Switzerland, 2011.

[9] M. Wobak, M. Gebhart, U. Muehlmann, "Physical limits of battery-less HF RFID transponders defined by system properties", in RFID-TA 2012.

[10] EMV® Contactless Specifications for Payment Systems, *Book D – EMV Contactless Communication Protocol Specification, V. 2.1.* EMVCo, LLC, March 2011.

[11] NFC Forum, *Consortium Homepage.* 401 Edgewater Place, Suite 600, Wakefield, MA 01880, USA: http://www.nfc-forum.org, 2012.

[12] ECMA356, *NFCIP-1 - RF Interface Test Methods*, June 2004

[13] R. Stadlmair and M. Gebhart, "Cadence Simulation Environment for Contactless Near-Field Communication tags", in Proc. of the 11th ConTEL, ISBN: 978-953-184-152-8, pp. 39-46, June 2011.

[14] M. Gebhart, "Analytical considerations for an ISO/IEC14443 compliant Smartcard", in ConTEL, pp. 9-16, June 2011.

[15] TF2 N723, "Active Transmission from Card to Reader", ISO/IEC JTC 1/SC 17/WG 08 "Integrated circuit cards without contacts", TF 2 meeting, Feb. 2012, Aix-en-Provence

[16] TF2 N738, "PICC Response Phase Drift Analysis and Measurement", ISO/IEC JTC 1/SC 17/WG 08 "Integrated circuit cards without contacts", TF 2 meeting, April 2012, Graz, Austria